SUPPORTING INFORMATION

Pieter Schipper, Marlies Hiemstra, Kari Bosch, Desiree Nieuwenhuis, Annalisa Adinolfi, Sabine Glotzbach, Bart Borghans, Dora Lopresto, Guillén Fernández, Floris Klumpers, Erno J Hermans, Karin Roelofs, Marloes JAG Henckens and Judith R Homberg. *The association between serotonin transporter availability and the neural correlates of fear bradycardia*

www.pnas.org/cgi/doi/10.1073/pnas.1904843116

SUPPORTING RESULTS

Experiment 1: Human Magnetic Resonance Imaging

Neural Activity: Main Effect of Threat and Threat x Genotype interaction

Threat anticipation (CS^+>CS^-) was associated with BOLD signal increases in a neural network encompassing the bilateral dorsal medial prefrontal cortex, anterior insula, ventral striatum / putative bed nucleus of the stria terminalis (BNST), and thalamus/midbrain (Supplementary Figure 1A), among other areas, but not the amygdala (Table S1) (1-3). As reported before (3), a genotype x threat interaction was observed in the dorsomedial prefrontal cortex (dmPFC). S-allele carriers displayed greater differential dmPFC activity to threat cues than LL homozygotes (Table 1, Fig. S1B). Previously, activation in this region was shown to mediate the increase in anticipatory psychophysiological reactions in S-allele carriers indexed by skin conductance and startle reaction (3). However, dmPFC activity did not correlate with fear bradycardia ($r_{(103)}$=0.052, p=0.601) and thus apparently did not underlie the observed exaggerated bradycardic response to threat in S-allele compared to LL-allele carriers. This is in line with previous reports on the association of activity in this region with sympathetic (instead of parasympathetic) responses, increased blood pressure, and HR acceleration (4, 5).

PAG Connectivity

Psychophysiological interaction (PPI) analysis to investigate PAG functional connectivity during the processing of threat revealed a significant increase in PAG connectivity to other regions within the midbrain and the right amygdala (Table 2), which was significantly greater in S-allele compared to LL-carriers (Fig. 2A, Table 2). *Post hoc* testing revealed a significant threat-induced increase in PAG-amygdala connectivity in the S-allele carriers, but not LL-carriers (no significant voxels, even at a more lenient threshold of p<0.05 uncorrected). This

effect appeared to be caused by increased PAG-amygdala connectivity during the processing of the threat cue in S-allele carriers; during threat processing S-allele carriers displayed increased PAG-amygdala coupling compared to fixation, unlike LL-allele carriers (no significant voxels, even at a more lenient threshold of $p<0.05$). No differences in PAG-amygdala connectivity between genotypes were observed in response to the safe cue.

Experiment 2: Neuronal Activity in Animal Model

Effect of 5-HTT Genotype on Neuronal Activity in the Prefrontal Cortex

The number of activated excitatory neurons (GAD67- and c-Fos+) in the IL was reduced in KO compared to WT rats ($F_{(1,33)}=7.992$, $p=0.008$). As excitatory projection neurons of the IL are involved in the regulation of fear expression (6, 7), we tested whether their activity mediated the effect of genotype on freezing behavior during threat re-exposure in conditioned rats. Although mediation analyses tended to confirm that 5-HTT KO rats show reduced IL excitatory neuronal activity (path *a*: coeff=4.77, $z=1.86$, $p=0.062$), no association between IL excitatory neuronal activity and exaggerated freezing during cooldown was observed (path *b*: coeff=-0.12, $z=-0.72$, $p=0.472$), nor did this activity mediate the 5-HTT effect on the fear response (path *ab*: coeff=-0.38, $z=-0.17$, $p=0.866$). Thus, excitatory activation in the IL did not mediate the relationship between 5-HTT genotype and fear responding.

As the human neuroimaging findings revealed a genotype x condition interaction in the dmPFC, we also assessed neuronal activity in the prelimbic (PrL) cortex, its supposed rodent homologue (8). No significant effects of genotype, condition or genotype x condition interaction were observed for neuronal activity observed in the PrL cortex of the rats (all *F*'s<1) (GABAergic activity; $WT_{control}=4.46\pm1.05$, $WT_{FC}=5.47\pm2.04$, $KO_{control}=4.97\pm2.08$, $KO_{FC}=4.93\pm1.81$; glutamatergic activity; Fig. S4a), nor was there a significant difference in

the amount of inhibitory neurons in this region between genotypes (F<1; WT=59.33±12.40, KO=61.61±7.39).

Effect of 5-HTT Genotype on Neuronal Activity in the PAG

Activity measures in the vlPAG (i.e., of CaMKII-expressing (putative glutamatergic) projection neurons, non-CaMKII expressing neurons (putative local GABAergic neurons), or their balance) were not modulated by condition or a condition x genotype interaction (all p's>0.23). No significant differences were observed in the amount of projection neurons in the vlPAG between genotypes ($F_{(1,27)}$=2.438, p=0.130; WT=10.47±7.24, KO=6.80±5.36).

Because of its involvement in mediating sympathetic stress responding and its inhibitory projections to the vlPAG, we also assessed activity in the dorsolateral PAG (dlPAG). Analysis of dlPAG c-Fos expression revealed no main effect of genotype, condition, or genotype x condition interaction (all p's>0.19) ($WT_{control}$=56.63±18.90, WT_{FC}=53.66±19.43, $KO_{control}$=48.02±9.79, KO_{FC}=59.65±11.21). There were also no differences between genotypes in the total amount of dlPAG CaMKII-expressing projection neurons ($F_{(1,28)}$=1; WT=17.30±11.37, KO=21.54±14.52). Neither the activity of dlPAG CaMKII+ neurons (F's<1, Fig. S4b), nor that of CaMKII- neurons (putative local GABAergic neurons), nor their balance in the dlPAG revealed main effects of genotype or condition, or condition x genotype interaction (all p's>0.19).

SUPPORTING METHODS

Experiment 1: Human Magnetic Resonance Imaging

Participants

Participants were recruited through advertisements posted around the Radboud University Medical Centre, Nijmegen, The Netherlands (104 male subjects). All subjects were aged 18 to 30 (mean±stdev: 21.9±2.5 years) and reported no regular use of psychoactive drugs or history of neurologic and psychiatric disorders (3). More than 90% of participants in the sample were of North European origin.

Genotyping

DNA was isolated from saliva using Oragene containers (DNA Genotek, Kanata, Ontario, Canada). 5-HTTLPR genotyping was performed using polymerase chain reaction followed by sequence length analysis using an automated capillary sequencer (ABI3730, Applied Biosystems Foster City, California) to classify each subject as having either two short 486 base pair DNA fragments (SS), one short and one long (529 base pair) fragment (SL), or two copies of the long fragment (LL) (3). To ensure sufficient power and in line with previous research (3, 9-12), short allele carriers (SS and SL) were contrasted statistically with LL homozygotes in all analyses.

Experimental Design

Participants were first asked to complete the Spielberger's trait anxiety inventory (13) and the NEO-Five Factor Inventory (FFI) Personality Inventory (14). Then, participants received instructions for the fear conditioning task in the MRI scanner. They were informed that they would see a yellow or blue square on a computer screen and that electrical shocks would be

administered. The level of the shocks, administered to the fingers, was set before the experiment to a subjective intensity that was maximally uncomfortable without being painful to the subject. Subjects were instructed to pay attention to the screen and were informed that a relationship existed between the stimuli and shocks. Colored squares were presented for 4 seconds in pseudorandomized order. Each stimulus was presented 18 times with an intertrial interval of 11-13 seconds. One square color co-terminated with the presentation of the electric shock stimulation on one third of the trials; the other color was never paired with electric stimulation (stimulus type counter-balanced across participants). Only no-shock trials were used for analyses to exclude reactions to the shocks.

Heart Rate Recording and Analysis

Cardiac rhythm of the participants was measured during scanning, using a pulse oximeter placed on their left index finger. Participants were instructed to keep their hands as still as possible during the measurement. Heart rate (HR) frequency was calculated using in-house software, and manually checked and corrected if necessary (i.e., in case of aberrant inter-beat intervals). HR responses to the presented stimuli (i.e., the threat (non-reinforced CS^{+}) and safe cues (CS^{-})) were calculated by subtracting baseline HR, defined as the average HR in the 11 second period prior to stimulus presentation, from the averaged HR observed during stimulus presentation (4 seconds). The fear bradycardia response used for analysis was defined as the difference in average HR response to threat vs. safe cues (ΔHR).

Magnetic Resonance Imaging

Magnetic resonance imaging (MRI) data were acquired on a 1.5 T Avanto MR scanner (Siemens, Erlangen, Germany) at the Donders Institute in Nijmegen, The Netherlands. A series of 302 T2*-weighted functional images were acquired using gradient echo-planar

imaging with the following parameters: 32 oblique transverse slices, voxel size=3.5×3.3×3.3 mm, repetition time (TR)=2.34 s, flip angle α=90°, echo time (TE)=35 ms. A three-dimensional (3-D) magnetization prepared rapid acquisition gradient-echo anatomical T1-weighted image was acquired for normalization purposes (176 slices, 1.0 mm isotropic, TR=2730 ms, TE=2.95 ms).

fMRI Data Analysis

Functional scans were realigned and subsequently co-registered to the anatomical scan to spatially normalize functional images via the anatomical scan to the Montreal Neurological Institute 152 T1-template image via the unified segmentation procedure in SPM8 (Wellcome Trust Centre for Neuroimaging, London, United Kingdom; http://www.fil.ion.ucl.ac.uk/spm/). The normalized images (3.5 mm isotropic) were then smoothed with an isotropic 3-D Gaussian kernel with a full-width at half maximum of 8 mm. In SPM, a general linear model was composed to relate blood oxygen level-dependent (BOLD) signal variation in each voxel to the task conditions. The predictors of neural activity were the threat conditions (CS^+), safe conditions (CS^-), and the shocks and these were modeled with 4-s boxcars with appropriate duration. Regressors were convolved with the canonical hemodynamic response function in SPM. Realignment parameters were included in the model as regressors of no interest. High-pass filtering (cutoff 128 seconds) and a first-order autoregressive model were used, which is the default in SPM. Reactions to CS^+ and CS^- were contrasted in each subject to index threat-related responses. The single subject contrast maps were subsequently subjected to random effects analyses. Due to fMRI data loss, one participant (S-carrier) was excluded from all fMRI analyses. Whole-brain results for the effects of threat were thresholded at the voxel-level at $p<0.05$ family-wise error (FWE) corrected for multiple comparisons according to random field theory implemented in SPM, whereas whole-brain cluster level $p<0.05$ FWE

correction was applied for the effect of genotype and genotype x threat (using an initial $p<0.005$ uncorrected clustering threshold). For correlational analysis, the mean beta weights were extracted from the specific clusters that showed a genotype effect. Based on the strong neurophysiological evidence for the involvement of the PAG in mediating fear bradycardia (15), the PAG was considered *a priori* a region of interest and the mean beta weights of the anatomically defined PAG (16) were extracted for statistical analyses. Visualizations of activations were created in SPM8 by superimposing statistical parametric maps thresholded at $p<0.005$ uncorrected (unless indicated otherwise) onto a canonical T_1-weighted image in a standard MNI 152 space.

Functional Connectivity Analysis: Psychophysiological Interaction

Psychophysiological interaction (PPI) analyses can be used to assess how activity in brain regions covaries with a source region in response to the experimental condition (17). We examined functional connectivity of the PAG as a source region to investigate whether 5-HTTLPR genotype affected its threat-related functional connectivity. To test this, we extracted the deconvolved time series from the anatomically defined PAG (16), (N.B. Analyses were repeated with the anatomic PAG mask as defined by Hashemi et al. (18) which generated similar results) and the PPI was calculated as the element-by-element product of the source region (the first eigenvariate from the time series of all voxels) and a vector coding for the effect of threat (the contrast "$CS^{+}>CS^{-}$"). This product was subsequently reconvolved with the hemodynamic response function, and the resulting interaction term was entered as a regressor in a first-level model together with the time series of the PAG and the vector coding for the effect of threat. The model was estimated and contrasts were generated to test the effects of positive and negative PPIs. This analysis identified regions that display stronger functional connectivity with the PAG during threat processing. Next, the contrast images for

the PPI effects were entered in a second-level analysis and tested for genotype effects using a two-sample t-test. Like for the conventional fMRI analyses, contrast maps were thresholded at $p<0.005$ uncorrected followed by whole brain FWE correction at the cluster-level of $p<0.05$. Based on the strong neurophysiological evidence for functional connections between the PAG and amygdala (19), involved in mediating the bradycardic response to threat (20, 21), the amygdala was considered *a priori* a region of interest and subjected to small-volume correction using its anatomical mask as defined by the WFU PickAtlas Tool (version 2.4, amygdala AAL mask). Statistical tests for the amygdala were FWE rate corrected ($p<0.05$) for multiple comparisons at the voxel level. For correlational analysis, we extracted the mean beta weight from the ROI.

Statistical Analysis of Behavioral and Physiological Data

Data are presented in the figures as mean ± standard error of the mean (SEM). Behavioral and physiological data were analyzed in IBM SPSS Statistics version 23.0 (SPSS Inc., Chicago, Illinois, USA) using independent samples and paired samples *t*-tests. For correlational analyses, Pearson correlations were used. To test whether genotype-dependent neural connectivity might mediate an impact of genotype on psychophysiological responses, we performed a mediation analysis with accelerated bias-corrected bootstrap significance testing (10,000 bootstrap samples) as implemented in the M3 toolbox (https://github.com/canlab) (22). Alpha was set at 0.05 throughout.

Experiment 2: Neuronal Activity in Animal Model

Animals

Whereas 5-HTT heterozygous rats closer resemble the human 5-HTTLPR S-allele carriers in terms of 5-HTT levels they, unlike 5-HTT KO rats (23, 24), do not show behavior that

resembles the human S-allele phenotype (25-27), indicating a dissimilar gene-dose effect of 5-HTT between species. Therefore, we considered the KO rat the preferred model for studying behavioral/neural/physiological measures of aberrant threat responding. Serotonin transporter knockout (5-HTT KO) rats were generated on a Wistar background by N-ethyl-N-nitrosurea (ENU)-induced mutagenesis and have been described previously (28). As controls we used wild-type (WT) littermates. 18 male, adult rats were used for HR recordings, and 40 male rats were used for immunohistochemistry. All animals had *ad libitum* access to food and water. A 12-hr light-dark cycle was maintained, with lights on at 08.00 AM. All behavioral experiments were performed between 08.00 AM and 18:00 PM. The animals were housed in pairs of the same genotype which were subjected to the same experimental protocol. Rats were habituated to handling for three weeks prior to the start of the experiment. All experiments were approved by the Committee for Animal Experiments of the Radboud University Nijmegen Medical Centre, Nijmegen, The Netherlands, and all efforts were made to minimize animal suffering and to reduce the number of animals used.

Procedure

Experiment 2 was designed to investigate the neuronal activation patterns underlying the mediation of threat anticipation and fear bradycardia by 5-HTT availability. In the human neuroimaging experiment, the relatively rapid dynamics of the BOLD-response allowed for the recording of the differential phasic neural responding to shock vs. threat vs. safety cues within a single subject and session. Unfortunately, the assessment of neuronal activation using immediate early gene expression (in human fMRI) lacks the required temporal resolution. Therefore, to be able to measure the neuronal response to threat anticipation, instead of actual shock delivery, rats were first exposed to Pavlovian fear conditioning (n_{KO}=19, n_{WT}=20), and then allowed to recover for 24 hours, until they were re-exposed to the conditioned cue (CS^{+})

in a novel environment. Then, their neural responses were compared to a control group (n_{KO}=10, n_{WT}=10) that was only exposed to the tones during conditioning (and not the shock delivery), to identify threat-related neuronal activation. The temporal separation of the conditioning and subsequent threat cue re-exposure 24 hrs later was also necessary to be able to distinguish the physiological response to threat anticipation vs. actual shock exposure, as these responses are much longer-lasting in animals (and thus do not recover in time) due to the relatively severe stressor implemented in these experiments. In order to measure HR responding, part of the conditioned animals (n_{KO}=9, n_{WT}=10) was equipped with a telemetric ECG transmitter.

Threat Cue Learning

Apparatus. Fear conditioning was performed in a 40.6 cm (width) x 15.9 cm (depth) x 21.3 cm (height) rectangular shuttle box (model ENV-010MD, Med Associates, St. Albans, VT, USA). The apparatus was split into two identical chambers by an automated door and housed within a sound-attenuating cubicle. The animals were placed in one of the compartments (the door kept closed), equipped with a speaker to produce an 85 dB 2.8 kHz tone. The grid floor of the apparatus was connected to a scrambled shock generator (model ENV-412, Med Associates, St. Albans, VT, USA).

Procedure. One day prior to conditioning, rats were placed in the fear conditioning box for 10 minutes to habituate to the novel environment. On the conditioning day, the rats were allowed to habituate for 2 minutes, after which they were exposed to three presentations of a 30 second 2880 HZ tone (the CS^{+}), that co-terminated with a one second 0.6 mA footshock, followed by a 60 second inter-trial interval. After these shocks, there was a 3 minutes cooldown period. In between animals, the cages were cleaned with 70 % EtOH.

Threat Cue Re-exposure

24 hours after conditioning, animals were re-exposed to the CS^+ in a novel environment. This novel environment comprised a 25 cm (width) x 25 cm (depth) x 35 cm (height) triplex box with an iron bottom covered with 1.5 cm of black sawdust. The walls of the boxes were covered with white paper to avoid the rat to observe the surrounding environment. The rats were first habituated in the novel environment for 7 minutes, after which the 2880 Hz tone was presented five times for 60 seconds, with a 60 second inter-trial interval. These threat cue presentations were followed by a 5-minute cooling down period.

During threat cue (CS^+) re-exposure, rats were videotaped and their freezing behavior was scored by a researcher blind to the condition and genotype of the rat with the help of ObserverXT_11 (Noldus, Wageningen, the Netherlands). Freezing data were analyzed in time bins, reflecting the habituation period (min 1-7), fear cue (tone) presentations (min 8, 10, 12, 14 and 16), inter-trials intervals (ITIs: min 9, 11, 13, 15), and cooldown period (min 17-20).

Heart Rate Recording and Analysis

Procedure. In a first batch of 19 animals, a telemetry ECG transmitter was implanted during a surgical procedure as described before (29). Briefly, anesthesia was induced using 5 % isoflurane and maintained on 2-3 % isoflurane. ECG transmitters (Data Sciences International™, type TA11CTA-F40, St. Paul, MN, USA) were implanted in the abdominal cavity with one electrode affixed to the dorsal side of the xiphoid process, and the other electrode subcutaneously attached near the salivary gland. After surgery, animals were isolated for 24 hours, after which they were reunited with their cage mate. Animals were allowed to recover for 14 days prior to the experiment, and carefully monitored throughout.

Apparatus. The radiotelemetry system consisted of an implantable transmitter with two flexible leads, a telemetric receiver (model RPC-1 and RLA1020), a Data Exchange Matrix

collecting input from the receivers and an in-line analogue ECG adaptor, all purchased from Data Sciences International™ (St. Paul, MN, USA). Signals from the transmitters were passed on via a radio signal to the receiver, localized under the behavioral apparatus, transforming it into a digital signal. Digital information from the telemetry receivers was collected by the data matrix and fed into the computer. Raw data were collected and analyzed by the software package Dataquest A.R.T. version 3.11 (Data Sciences International™, St. Paul, MN, USA).

Data Acquisition. HR (via electrocardiogram, ECG) was measured for each individual rat and exported every 10 seconds as the average of the last 5 seconds using DataQuest LabPRO (Version 3.11, Data Science International Technologies). Telemetry probe transmissions were recorded via Data Sciences International Technologies' PhysioTel Receiver Model RPC-1.

Data Analysis. The data received from the telemetry probe during fear cue re-exposure were collected. HR during the five cue presentations was measured and compared to baseline HR during the preceding habituation period. The bradycardic response used for analysis was defined as the average difference in HR during the processing of the threat cues from baseline (ΔHR), where stronger negative values indicate stronger fear bradycardia.

Immunohistochemistry

Procedure. A second batch of 40 animals (conditioned: n_{KO}=10, n_{WT}=10, control: n_{KO}=10, n_{WT}=10) was anesthetized by *i.p.* injection with pentobarbital and sacrificed at ~90 min after the first fear cue presentation by perfusion fixation with 4 % paraformaldehyde (PFA) in 0.1 M phosphate-buffered saline (PBS: pH 7.4). The brains were removed and post-fixed for 24 hours in 4 % PFA, after which they were stored in 0.1 M PBS. Next, the brains were cut by a sliding microtome (Microm HM-440-E, GMI, Minnesota, USA) in 30 μm thick slices.

Immunostainings focused on the regions of interest as provided by the findings obtained in experiment 1, i.e., the medial prefrontal cortex (mPFC), amygdala, and PAG. For the analysis of the mPFC, three slices (Bregma 3.2:2.7 mm) were selected for immunohistochemistry. Slices were first washed 4 times for 10 minutes in PBS. Sections were then blocked using PBS-containing 0.1 % bovine serum albumin and 0.03 % Triton X-100. To identify neuronal activity by means of the immediate early gene *Fos*, mPFC slices were incubated with the primary antibody rabbit anti-c-Fos (1:1000, sc-52, Santa Cruz Biotechnology, Heidelberg, Germany). Moreover, to determine the inhibitory (i.e., local GABAergic neurons) nature of the activated neurons, mPFC slices were simultaneously incubated with the primary antibody mouse anti-GAD67 (1:2000, MAb5406, Merck Millipore, Amsterdam, The Netherlands), labeling all GABAergic neurons. Markers for glutamatergic cell populations (guinea pig anti-vglut2, 1:1600, AB2251-I, Merck Millipore, Amsterdam, The Netherlands, and mouse anti-CaMKII, 1:500, SC-32288, Santa Cruz Biotechnology, Heidelberg, Germany) did however not induce clear labeling of glutamatergic soma in the infralimbic cortex (Fig. S5). Thus, dual labelling of the mPFC allowed us to identify the activation of inhibitory (GAD67 and c-Fos double-positive cells), whereas we relied on the absence of GAD67-expression as indicator of glutamatergic activity (c-Fos positive cells negative for GAD67 expression) (30). Potential significant contributions of non-neuronal sources of c-Fos expression were assessed by pilot experiments revealing that 97-98% of all c-Fos positive nuclei co-localized with the neuronal marker NeuN, suggesting minimal contribution of non-neuronal sources. The primary antibodies were diluted in blocking solution and slices were incubated overnight at room temperature, after which they were washed three times in PBS. Subsequently, all slices were incubated with secondary antibody for three hours (1:200 in blocking solution); anti-rabbit (Alexa 488, A21206, Thermo Fisher Scientific Inc, Waltham, MA, USA), and anti-mouse (Alexa 555, A31570, Thermo Fisher Scientific Inc, Waltham, MA, USA). The sections where

then washed three times in PBS, and mounted on gelatin-coated slides using Fluorsave (345789, Merck Millipore, Amsterdam, The Netherlands).

Similarly, three slices were selected of the amygdala (Bregma -1.92:-3.00 mm). Immunostainings were performed according to the same protocol as described for the mPFC, but using different antibodies, except for the rabbit anti-c-Fos antibody. Instead of labelling all GABAergic interneurons by use of anti-GAD67, amygdala slices were specifically labelled for somatostatin (SOM). Within the central amygdala (CeA) SOM+ neurons are known to project to the vlPAG (19, 31) and thereby modulate freezing behavior (32, 33). Thus, amygdala slices were incubated with both rabbit anti-c-Fos and mouse anti-somatostatin (1:200, SOM-018, GeneTex, Inc., Irvine, USA). An additional tyrosine hydroxylase primary antibody (chicken anti-TH, 1:1000, ab76442, Abcam, Cambridge, UK) was added to allow for a more reliable dissection of the amygdala subnuclei (34, 35). As secondary antibodies anti-rabbit Alexa 488, anti-mouse Alexa 555 and anti-chicken Alexa 647 (1:200, A21449, Thermo Fisher Scientific Inc, Waltham, MA, USA) were used.

Additionally, five PAG slices that included the vlPAG at different locations at the rostrocaudal axis, ranging from Bregma -6.72:-8.04 mm, were selected for immunohistochemistry. As previous research has indicated that GABAergic interneurons within the PAG inhibit glutamatergic projection neurons mediating freezing (32, 33), it was critical to distinguish activated GABAergic interneurons vs. glutamatergic projection neurons in the PAG. However, the GAD67-antibody effective in labelling cortical GABAergic neurons yielded only minimal labelling of PAG neurons (Fig. S6), which was contradictory to literature (31, 36). Therefore, we used the marker CaMKII in the PAG instead. Whereas CaMKII is most abundantly expressed in glutamatergic neurons (37, 38), recent reports have also indicated its expression in GABAergic projection neurons (39). This leaves the exact nature of these CaMKII-expressing projection cells unresolved, since the vlPAG also seems to

contain a minority of GABAergic projection neurons (40, 41). An identical staining protocol as for the prefrontal cortex and amygdala was implemented, using mouse anti-CaMKII (1:500, SC-32288, Santa Cruz Biotechnology, Heidelberg, Germany), rabbit anti-c-Fos (1:1000, 226003, Synaptic Systems, Goettingen, Germany), and chicken anti-NeuN (1:1000, ABN91, Merck Millipore, Amsterdam, The Netherlands) as primary antibodies, and goat anti-mouse Alexa 488 (A11001, Thermo Fisher Scientific Inc, Waltham, MA, USA), anti-rabbit Alexa 647 (A21245, Thermo Fisher Scientific Inc, Waltham, MA, USA) and anti-chicken Alexa 555 (A21437, Thermo Fisher Scientific Inc, Waltham, MA, USA) as secondary antibodies. After mounting the slices on gelatin coated slides using Fluorsave and drying overnight at RT in the dark, all slices were stored at -20°C.

Data Acquisition. Images were collected using a Leica CTR7000 HS fluorescence microscope (Leica Microsystems, Wetzlar, Germany) with a 20x-objective. Of the mPFC slices, two areas of 1782 by 1478 pixels were selected to represent the infralimbic (IL) and prelimbic (PrL) cortex using the rat brain atlas (Fig. S7) (42). For the amygdala, a circular area (that was adjusted in size to fit the anatomical landmarks) was selected to represent the central nucleus of the amygdala. Anatomical landmarks, i.e., the external capsule and stria terminalis' fiber tracts, visualized using the TH-signal, were used to place these ROIs (Fig. S3). For the PAG, three slices were selected at very similar location across the rostrocaudal axis (reflecting Bregma -6.84:-7.80 mm) for further analyses. ROIs for the ventrolateral and dorsolateral PAG were drawn based on anatomical landmarks (Fig. S8). Cell counting was done manually with the help of the Cell Counter (version 2010) plugin for ImageJ (de Vos, University of Sheffield, Academic Neurology) by researchers blind to the condition and genotype of the animals. Cells were counted positive if their morphology matched the expected morphology of a soma (for GAD67, CaMKII) or a nucleus (for c-Fos).

Data Analysis. Co-expression was identified by a c-Fos stained nucleus that fitted into a GAD67+/CaMKII+ soma. c-Fos positive cells in the mPFC that were negative for GAD67 were considered glutamatergic neurons. Potential non-neuronal contribution to c-Fos signal in the PAG was assessed as well, but was restricted to 1% of the cells. Including only c-Fos+ neurons did not change any of the results, which is why, for consistency with mPFC analyses, all c-Fos counts were included for analyses. Absolute cell counts were analyzed for the mPFC regions, whereas amygdalar and PAG counts were corrected for the ROI surface area (normalized to the overall average). For the PAG, the relative balance of regulating local inhibitory activity and that of glutamatergic output is critical for the maintenance of homeostasis (43, 44), making that we calculated the relative contribution of CaMKII-expressing projection neurons to overall PAG activity (i.e., (number of CaMKII+/c-Fos+ cells) / (number of CaMKII-/c-Fos+ cells)*100%).

Immunostainings for somatostatin failed in two rats (FC group: 1 KO, 1 WT), and for CaMKII in 5 more rats (FC group: 1 KO, 2 WTs, control group: 1 KO, 1 WT), due to suboptimal brain perfusion. Data were averaged to obtain a single measure per animal for further statistical analyses.

Statistical Analyses of Behavioral, Physiological and Neuronal Activation Data

Data are presented in the figures as mean ± SEM. All statistical analyses were performed using IBM SPSS Statistics version 23.0 (SPSS Inc., Chicago, Illinois, USA). Behavioral and physiological data were analyzed using repeated measures ANOVAs, followed up by independent *t*-tests. The immunohistochemical data were analyzed using a two-way ANOVA, implementing condition and genotype as between-subject factors. For correlational analyses, Pearson correlations were used. Finally, to test whether genotype-dependent neural activity and connectivity mediated an impact of genotype on psychophysiological responses, we

performed a mediation analysis with accelerated bias-corrected bootstrap significance testing (10,000 bootstrap samples) as implemented in the M3 toolbox (https://github.com/canlab) (22). Data points that deviated more than 2 standard deviations from the mean were considered as outliers and excluded from analyses. Alpha was set at 0.05 throughout.

SUPPORTING REFERENCES

1. Mechias ML, Etkin A, & Kalisch R (2010) A meta-analysis of instructed fear studies: implications for conscious appraisal of threat. *Neuroimage* 49(2):1760-1768.
2. Klumpers F, Kroes MCW, Baas JMP, & Fernandez G (2017) How Human Amygdala and Bed Nucleus of the Stria Terminalis May Drive Distinct Defensive Responses. *J Neurosci* 37(40):9645-9656.
3. Klumpers F*, et al.* (2015) Dorsomedial Prefrontal Cortex Mediates the Impact of Serotonin Transporter Linked Polymorphic Region Genotype on Anticipatory Threat Reactions. *Biol Psychiatry* 78(8):582-589.
4. Gray MA*, et al.* (2007) A cortical potential reflecting cardiac function. *Proc Natl Acad Sci U S A* 104(16):6818-6823.
5. Critchley HD, Corfield DR, Chandler MP, Mathias CJ, & Dolan RJ (2000) Cerebral correlates of autonomic cardiovascular arousal: a functional neuroimaging investigation in humans. *J Physiol* 523 Pt 1:259-270.
6. Amir A, Amano T, & Pare D (2011) Physiological identification and infralimbic responsiveness of rat intercalated amygdala neurons. *J Neurophysiol* 105(6):3054-3066.
7. Do-Monte FH, Manzano-Nieves G, Quinones-Laracuente K, Ramos-Medina L, & Quirk GJ (2015) Revisiting the role of infralimbic cortex in fear extinction with optogenetics. *J Neurosci* 35(8):3607-3615.
8. Gass JT & Chandler LJ (2013) The Plasticity of Extinction: Contribution of the Prefrontal Cortex in Treating Addiction through Inhibitory Learning. *Front Psychiatry* 4:46.
9. Lonsdorf TB & Kalisch R (2011) A review on experimental and clinical genetic associations studies on fear conditioning, extinction and cognitive-behavioral treatment. *Transl Psychiatry* 1:e41.
10. Klumpers F, Heitland I, Oosting RS, Kenemans JL, & Baas JM (2012) Genetic variation in serotonin transporter function affects human fear expression indexed by fear-potentiated startle. *Biol Psychol* 89(2):277-282.
11. Klucken T*, et al.* (2013) The 5-HTTLPR polymorphism is associated with altered hemodynamic responses during appetitive conditioning. *Hum Brain Mapp* 34(10):2549-2560.
12. Drabant EM*, et al.* (2012) Neural mechanisms underlying 5-HTTLPR-related sensitivity to acute stress. *Am J Psychiatry* 169(4):397-405.
13. van der Ploeg HM, Defares PB, & Spielberger CD (1980) *Handleiding bij de Zelf-Beoordelings Vragenlijst, ZBV: Een Nederlandse vertaling van de Spielberger State—Trait Anxiety Inventory* (Swets and Zeitlinger, Lisse, The Netherlands).
14. Piedmont RL, McCrae RR, & Costa PT, Jr. (1992) An assessment of the Edwards Personal Preference Schedule from the perspective of the five-factor model. *J Pers Assess* 58(1):67-78.
15. Koba S, Inoue R, & Watanabe T (2016) Role played by periaqueductal gray neurons in parasympathetically mediated fear bradycardia in conscious rats. *Physiol Rep* 4(12).
16. Coulombe MA, Erpelding N, Kucyi A, & Davis KD (2016) Intrinsic functional connectivity of periaqueductal gray subregions in humans. *Hum Brain Mapp* 37(4):1514-1530.
17. Friston KJ*, et al.* (1997) Psychophysiological and modulatory interactions in neuroimaging. *Neuroimage* 6(3):218-229.
18. Hashemi MM*, et al.* (in press) Neural Dynamics of Shooting Decisions and the Switch from Freeze to Fight. . *Sci Rep*.

19. Penzo MA, Robert V, & Li B (2014) Fear conditioning potentiates synaptic transmission onto long-range projection neurons in the lateral subdivision of central amygdala. *J Neurosci* 34(7):2432-2437.
20. Lojowska M, Ling S, Roelofs K, & Hermans EJ (2018) Visuocortical changes during a freezing-like state in humans. *Neuroimage* 179:313-325.
21. Hermans EJ, Henckens MJ, Roelofs K, & Fernandez G (2013) Fear bradycardia and activation of the human periaqueductal grey. *Neuroimage* 66:278-287.
22. Wager TD, Davidson ML, Hughes BL, Lindquist MA, & Ochsner KN (2008) Prefrontal-subcortical pathways mediating successful emotion regulation. *Neuron* 59(6):1037-1050.
23. Homberg JR & van den Hove DL (2012) The serotonin transporter gene and functional and pathological adaptation to environmental variation across the life span. *Prog Neurobiol* 99(2):117-127.
24. Kalueff AV, Olivier JD, Nonkes LJ, & Homberg JR (2010) Conserved role for the serotonin transporter gene in rat and mouse neurobehavioral endophenotypes. *Neurosci Biobehav Rev* 34(3):373-386.
25. Homberg JR, Schubert D, Asan E, & Aron EN (2016) Sensory processing sensitivity and serotonin gene variance: Insights into mechanisms shaping environmental sensitivity. *Neurosci Biobehav Rev* 71:472-483.
26. Homberg JR, Schubert D, & Gaspar P (2010) New perspectives on the neurodevelopmental effects of SSRIs. *Trends Pharmacol Sci* 31(2):60-65.
27. Schipper P, Henckens M, Lopresto D, Kozicz T, & Homberg JR (2018) Acute inescapable stress alleviates fear extinction recall deficits caused by serotonin transporter abolishment. *Behav Brain Res* 346:16-20.
28. Smits BM*, et al.* (2006) Generation of gene knockouts and mutant models in the laboratory rat by ENU-driven target-selected mutagenesis. *Pharmacogenet Genomics* 16(3):159-169.
29. Sgoifo A*, et al.* (1996) Electrode positioning for reliable telemetry ECG recordings during social stress in unrestrained rats. *Physiol Behav* 60(6):1397-1401.
30. Ritov G, Boltyansky B, & Richter-Levin G (2016) A novel approach to PTSD modeling in rats reveals alternating patterns of limbic activity in different types of stress reaction. *Mol Psychiatry* 21(5):630-641.
31. Tovote P*, et al.* (2016) Midbrain circuits for defensive behaviour. *Nature* 534(7606):206-212.
32. Yu K, Garcia da Silva P, Albeanu DF, & Li B (2016) Central Amygdala Somatostatin Neurons Gate Passive and Active Defensive Behaviors. *J Neurosci* 36(24):6488-6496.
33. Fadok JP*, et al.* (2017) A competitive inhibitory circuit for selection of active and passive fear responses. *Nature* 542(7639):96-100.
34. Chieng BC, Christie MJ, & Osborne PB (2006) Characterization of neurons in the rat central nucleus of the amygdala: cellular physiology, morphology, and opioid sensitivity. *J Comp Neurol* 497(6):910-927.
35. Chieng B & Christie MJ (2010) Somatostatin and nociceptin inhibit neurons in the central nucleus of amygdala that project to the periaqueductal grey. *Neuropharmacology* 59(6):425-430.
36. Sapin E*, et al.* (2009) Localization of the brainstem GABAergic neurons controlling paradoxical (REM) sleep. *PLoS One* 4(1):e4272.
37. Benson DL, Isackson PJ, Gall CM, & Jones EG (1992) Contrasting patterns in the localization of glutamic acid decarboxylase and Ca2+/calmodulin protein kinase gene expression in the rat central nervous system. *Neuroscience* 46(4):825-849.

38. Jones EG, Huntley GW, & Benson DL (1994) Alpha calcium/calmodulin-dependent protein kinase II selectively expressed in a subpopulation of excitatory neurons in monkey sensory-motor cortex: comparison with GAD-67 expression. *J Neurosci* 14(2):611-629.
39. Dedic N*, et al.* (2018) Chronic CRH depletion from GABAergic, long-range projection neurons in the extended amygdala reduces dopamine release and increases anxiety. *Nat Neurosci* 21(6):803-807.
40. Ntamati NR, Creed M, Achargui R, & Luscher C (2018) Periaqueductal efferents to dopamine and GABA neurons of the VTA. *PLoS One* 13(1):e0190297.
41. Reichling DB & Basbaum AI (1990) Contribution of brainstem GABAergic circuitry to descending antinociceptive controls: I. GABA-immunoreactive projection neurons in the periaqueductal gray and nucleus raphe magnus. *J Comp Neurol* 302(2):370-377.
42. Paxinos G & Watson C (1998) *The Rat Brain in Stereotaxic Coordinates.* (Academic Press, Cambridge, MA).
43. Schmidtko A*, et al.* (2008) Genetic deletion of synapsin II reduces neuropathic pain due to reduced glutamate but increased GABA in the spinal cord dorsal horn. *Pain* 139(3):632-643.
44. Siegfried B & de Souza RL (1989) NMDA receptor blockade in the periaqueductal grey prevents stress-induced analgesia in attacked mice. *Eur J Pharmacol* 168(2):239-242.

SUPPORTING TABLES

Table S1. Peak voxels and corresponding *t* values of significantly activated clusters in the main effect of fear conditioning

Brain region	Cluster size	MNI coordinates			Peak
		x	y	z	T-value
$CS^+ > CS^-$					
Extended activation cluster covering the bilateral anterior insula, postcentral gyrus, superior temporal gyrus, BNST, thalamus and brain stem (PAG)	7551***	-28	26	4	10.98
Supplementary motor area, L	3476***	-4	-4	50	9.72
	1*	-8	-6	66	6.83
Supplementary motor area, R	2*	2	-8	68	7.01
	1*	16	2	66	6.13
Precentral gyrus, L	1538***	-34	-12	60	9.52
Supramarginal gyrus, L	1186***	-58	-24	24	8.40
Supramarginal gyrus, R	1597***	58	-40	24	8.37
Inferior parietal lobe, R	14**	40	-46	40	5.31
Middle frontal gyrus, R	749***	42	2	40	7.75
	49***	30	42	22	5.84
Middle cingulate cortex, R	54***	12	-24	42	5.77
Middle temporal gyrus, L	2*	-50	-52	8	4.90
Insular lobe, L	1*	-36	-20	16	4.84
Putamen, R	1*	24	10	2	4.81
$CS^+ < CS^-$					
Extended cluster covering the bilateral lingual gyrus and precuneus	8068***	12	-52	2	9.64
Precuneus, L	1*	-4	-56	42	4.83
Angular gyrus, L	601***	-44	-66	32	8.45
Middle occipital gyrus, R	31**	48	-78	10	5.30
Middle temporal gyrus, R	42***	58	-62	22	5.54
	6*	66	-4	-18	5.14

Middle temporal gyrus, L	103***	-62	-8	-16	5.86
	2*	-58	-2	-24	4.82
	1*	-56	-4	-26	4.81
Middle frontal gyrus, L	13**	-34	16	52	5.06
Superior frontal gyrus, L	470***	-10	56	36	6.68
Superior medial gyrus, L	189***	-4	62	8	5.94
Middle orbital gyrus, R	7*	2	60	-4	4.96
Rectal gyrus, L	2*	0	34	-18	4.91
	3*	-2	46	-16	4.87

MNI, Montreal Neurological Institute; R, right; L, left. All effects are analyzed using cluster-level statistics, implementing a height threshold at $p<0.05$ family wise error (FWE) corrected at the voxel level. ***: $p<0.001$; **: $p<0.01$; *: $p<0.05$

Table S2. All peak voxels and corresponding *t* values of significant clusters in the psychophysiological interaction (PPI) analysis seeding the periaqueductal grey

Brain region	Cluster size (cm^3)	MNI coordinates x	y	z	Peak T-value
$CS^+ > CS^-$					
Brain stem	27.70**	-10	-22	-18	4.29
$CS^+ < CS^-$	/				
5-HTTLPR S-carrier ($CS^+ > CS^-$) > 5-HTT LL-carrier ($CS^+ > CS^-$)					
Amygdala, R	1.93	30	-2	-18	4.06$^{\#\#}$
Amygdala, L	0.77	-28	4	-18	3.97$^{\#\#}$
S-carrier ($CS^+ > CS^-$)					
Amygdala, R	5.45	30	-4	-14	3.97$^{\#\#}$
Amygdala, L	3.26	-26	4	-18	3.90$^{\#\#}$
LL-carrier ($CS^+ > CS^1$)	/				
S-carrier ($CS^+ >$ fixation)					
Amygdala, R	5.49	32	-2	-16	5.22$^{\#\#\#}$
Amygdala, L	5.36	-26	-4	-22	4.79$^{\#\#\#}$
LL-carrier ($CS^+ >$ fixation)	/				
5-HTTLPR S-carrier ($CS^+ < CS^-$) > 5-HTTLPR LL-carrier ($CS^+ < CS^-$)					
Superior temporal / supramarginal gyrus, R	17.66*	32	-40	22	3.90

MNI, Montreal Neurological Institute; R, right; L, left. All effects are analyzed using a height threshold at $p<0.005$ uncorrected at the voxel level. **: $p<0.01$; *: $p<0.05$; $^{\#\#}$: $p<0.01$; $^{\#\#\#}$: $p<0.001$ small-volume corrected at voxel-level

Table S3. Supporting results on 5-HTT KO vs WT rats

Outcome parameter	**Mean±SD**
GAD67+ neurons in IL	WT: 56.61±5.73 KO: 51.21±8.70
GAD67+/cFos+ neurons in IL	$WT_{control}$: 3.93±1.51 WT_{FC}: 5.35±2.41 $KO_{control:}$ 3.43±1.40 KO_{FC}: 3.50±1.21
SOM+ neurons in CeA	WT: 517.44±117.09 KO: 582.20±104.66
CaMKII-/cFos+ neurons in vlPAG	WT: 51.07±19.34 KO: 65.96±21.90

CeA: central amygdala, IL: infralimbic cortex, SD: standard deviation, vlPAG: ventrolateral periaqueductal grey

SUPPORTING FIGURES

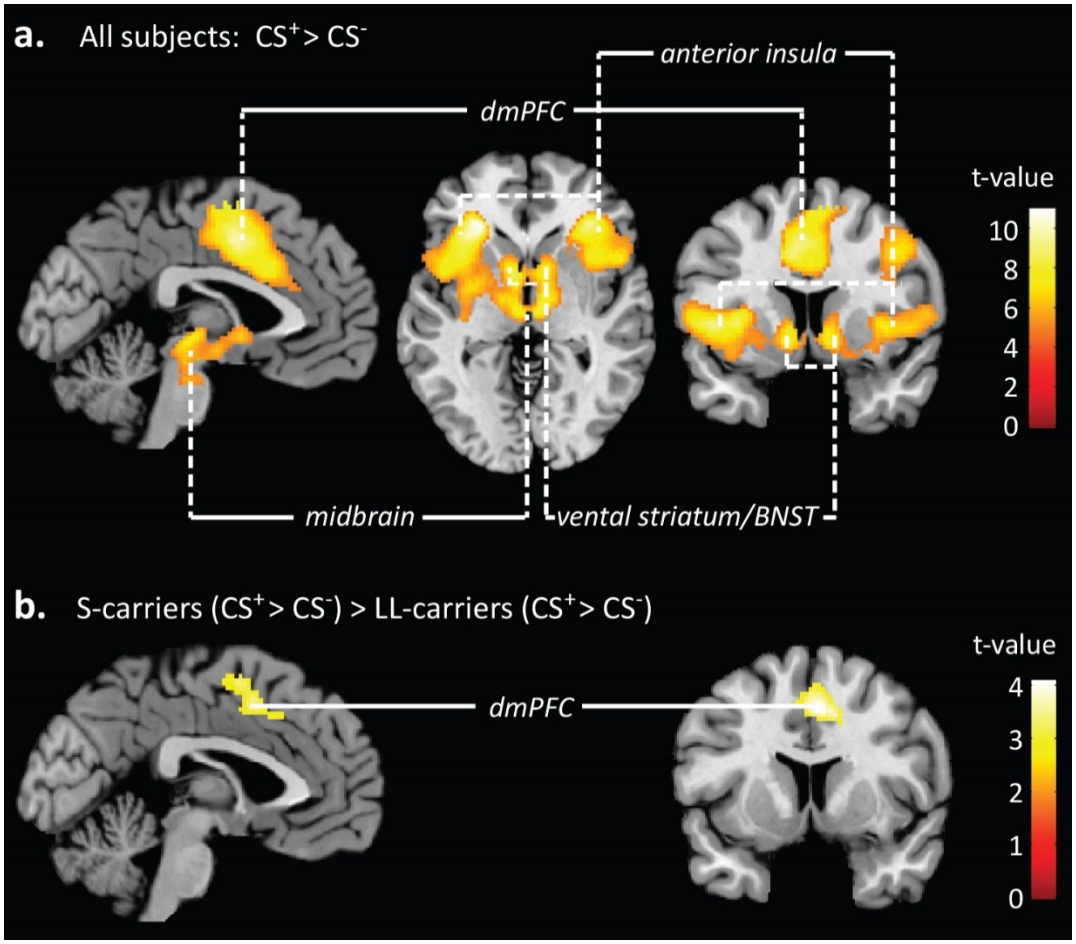

Fig. S1. Threat-related neuronal processing and its modulation by 5-HTTLPR genotype. **(a)** Processing of the threat-related cue (CS^+) induced increased activity in a neural network encompassing the bilateral dorsomedial prefrontal cortex (dmPFC), anterior insula, ventral striatum/bed nucleus of the stria terminalis (BNST), and thalamus/midbrain compared to the processing of a safe cue (CS^-). **(b)** S-allele carriers displayed increased threat-related processing in a cluster within the dorsomedial prefrontal cortex (3).

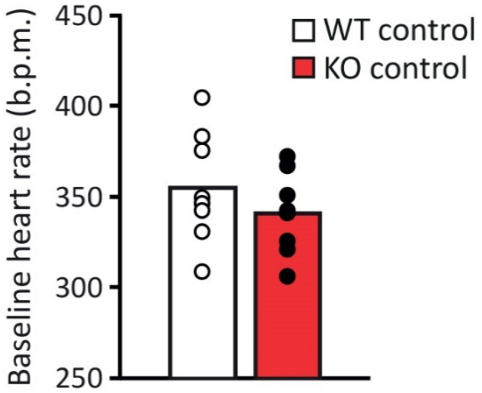

Fig. S2. Baseline heart rate in 5-HTT wildtype (WT) and knockout (KO) rats. Basal heart rate was not different in a separate batch of WT and KO rats that was not exposed to fear conditioning.

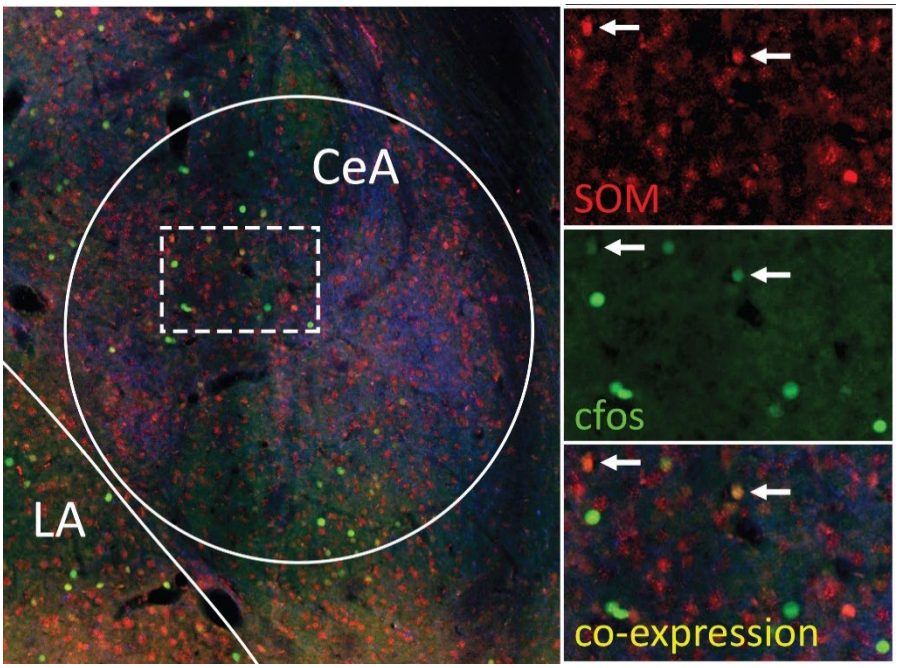

Fig. S3. Activity of somatostatin (SOM)-expressing neurons in the central amygdala (CeA) was assessed by immunostaining for SOM and the immediate early gene marker c-Fos. Additional staining for tyrosine hydroxylase (in blue) allowed for more reliable dissection of the amygdala subnuclei (lateral amygdala (LA) and CeA). Co-expression of c-Fos and SOM indicated activity of vlPAG projection neurons (marked by arrows).

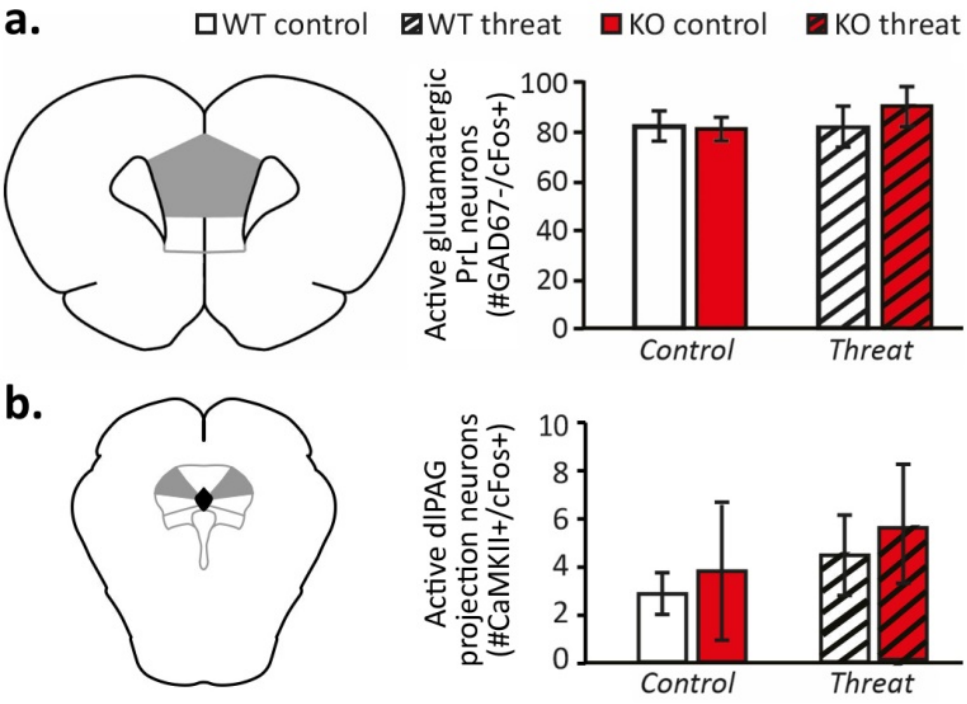

Fig. S4. No significant differences between 5-HTT knock out (KO) and wildtype (WT) rats were observed in the activity of glutamatergic neurons in the prelimbic cortex (PrL) (approximated by the number of GAD67-/cFos+ cells) **(a)** and CaMKII-expressing projection neurons in the dorsolateral periaqueductal grey (dlPAG) **(b)**.

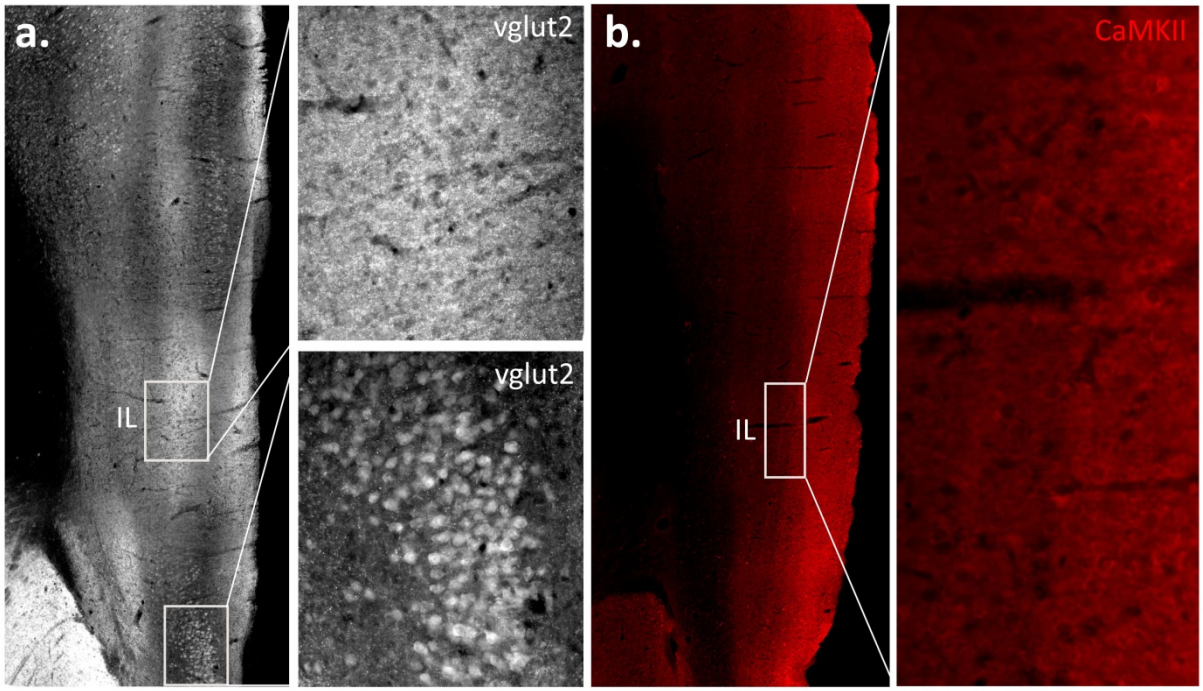

Fig. S5. Immunohistochemical stainings for glutamatergic markers Vglut2 **(a)** and CaMKII **(b)** did not allow for the identification of clear glutamatergic soma in the infralimbic cortex (IL).

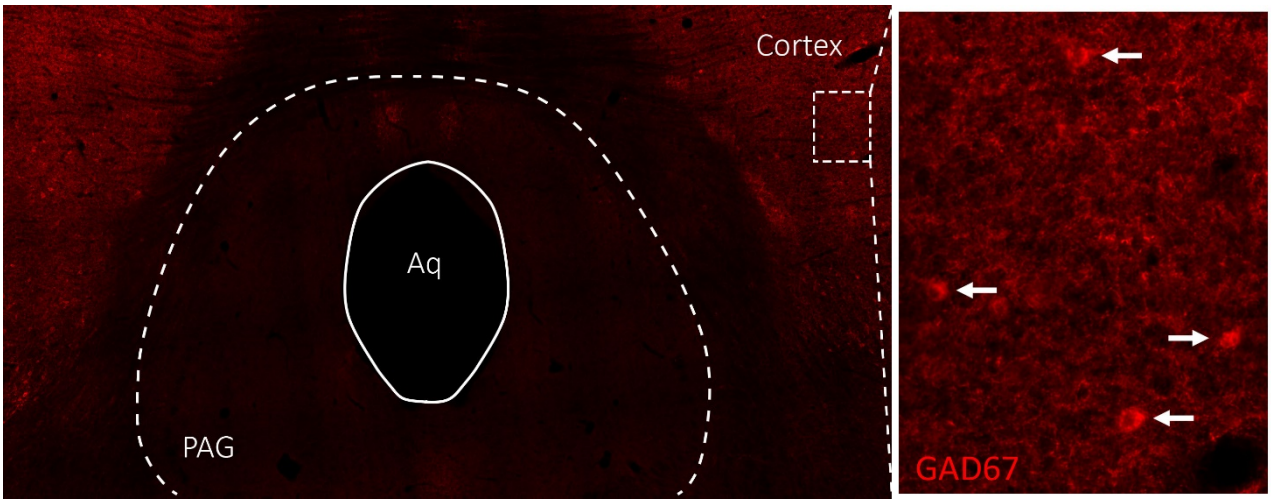

Fig. S6. Immunostaining for GAD67 only yielded minimal cell labelling within subcortical brain regions (the periaqueductal grey (PAG) is shown), whereas clear labelling of GABAergic neurons was observed in cortical areas. Aq: aquaduct

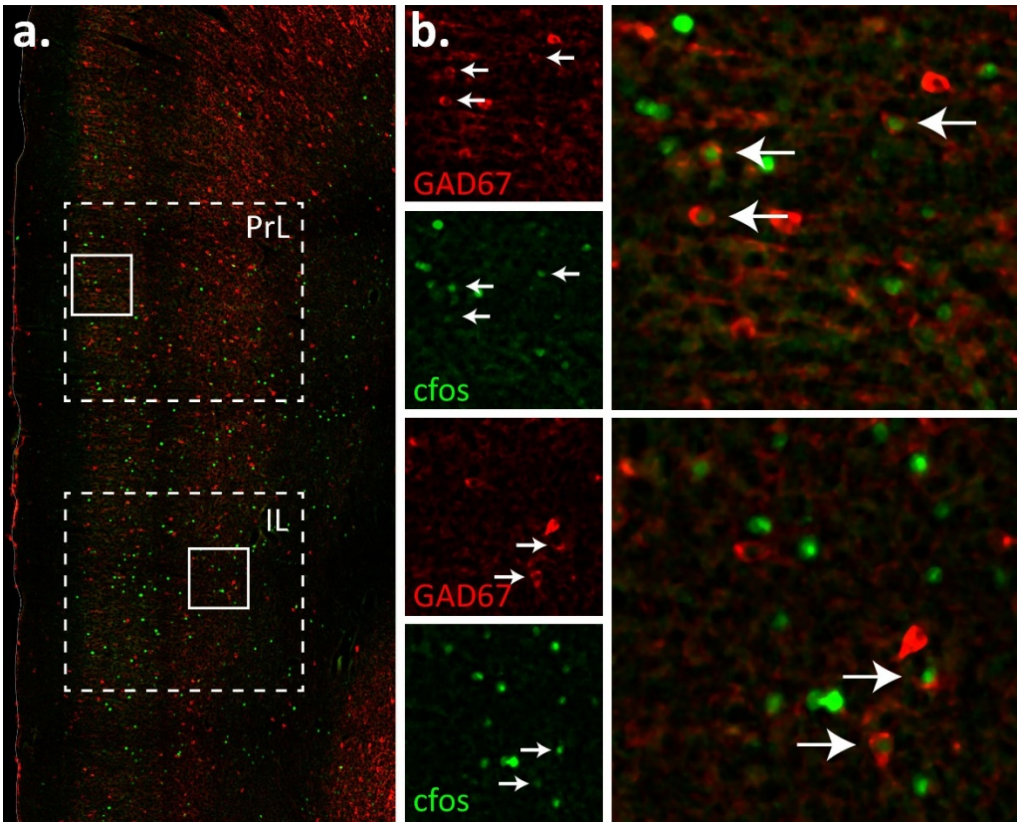

Fig. S7. (a) Activity of GABAergic neurons within the prelimbic (PrL) and infralimbic (IL) cortex was assessed by immunostaining for the immediate early gene marker c-Fos in combination with the GABAergic marker GAD67. **(b)** High magnification inserts reveal clear co-localisation of c-Fos and GAD67 expression, indicating GABAergic activity (marked by arrows). C-Fos positive cells that did not co-localize with GAD67 were considered to be glutamatergic.

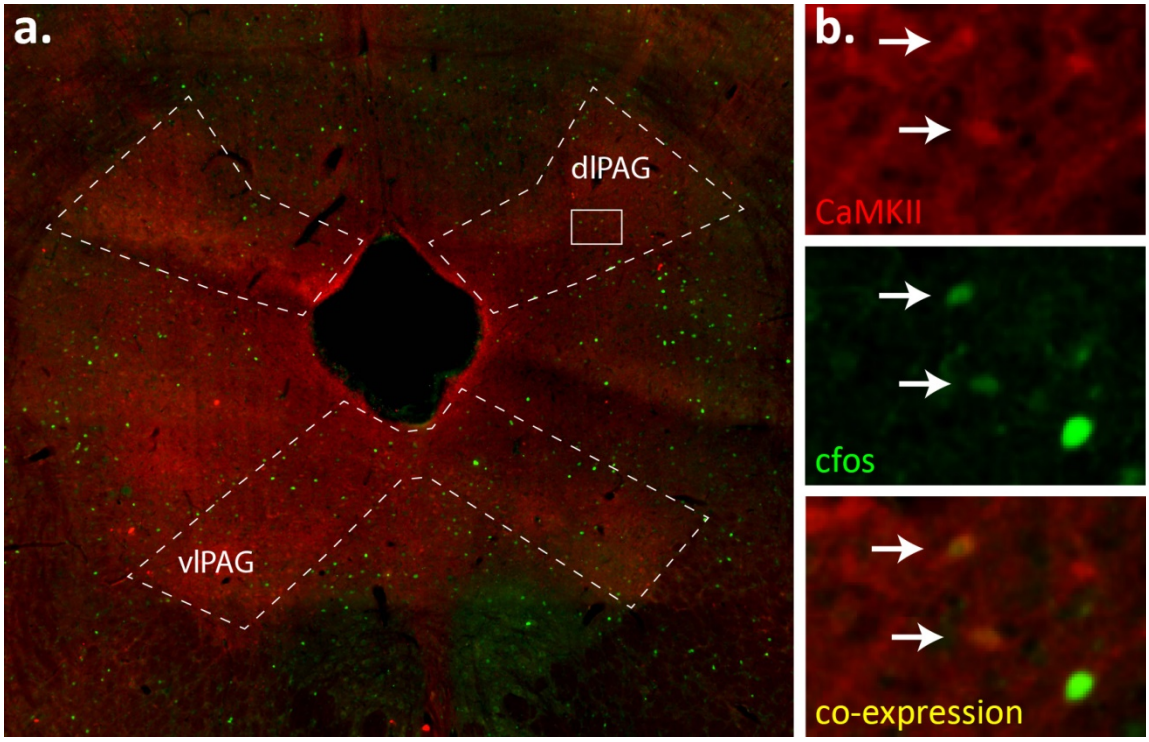

Fig. S8. (a) Activity of CaMKII-expressing projection neurons within the ventrolateral periaqueductal grey (vlPAG) and dorsolateral periaqueductal grey (dlPAG) was assessed by immunostaining for the immediate early gene marker c-Fos in combination with the marker CaMKII. **(b)** High magnification inserts reveal clear co-localisation of c-Fos and CaMKII expression, indicating activity of (CaMKII-expressing) projection neurons (marked by arrows). C-Fos positive cells that did not co-localize with CaMKII reflect putative GABAergic interneurons.